The relative roles of the South China Sea summer monsoon and ENSO in the Indian Ocean dipole development

Yazhou Zhang[1] · Jianping Li[1,2] · Jiaqing Xue[3] · Fei Zheng[4] · Renguang Wu[5] · Kyung-Ja Ha[6,7] · Juan Feng[1]

Abstract

The influence of El Niño-Southern Oscillation (ENSO) on the Indian Ocean Dipole (IOD), a coupled ocean–atmosphere mode of interannual climate variability, has been widely investigated over recent decades. However, a latest study indicates that the South China Sea summer monsoon (SCSSM) might also be responsible for IOD formation. Furthermore, an abnormal SCSSM does not always coincide with ENSO during boreal summer (June–August, JJA); consequently, the individual and combined effects of the SCSSM and ENSO on the IOD remain elusive. This study shows that the amplitude of the IOD tends to be much stronger under the coexistence of SCSSM and ENSO than that under individual SCSSM or ENSO events during JJA and autumn. The findings also indicate that the SCSSM and ENSO play the dominant role around the eastern and western poles of the IOD, respectively. An anomalous local Hadley circulation closely related to the stronger SCSSM favors anomalous southeasterly off Sumatra and Java during JJA, which enhance oceanic upwelling and subsequently result in cooling of the sea surface temperature (SST) over this area. Similarly, it can be envisaged that the contemporaneous ENSO could influence JJA SST anomalies over the western Indian Ocean via the Walker circulation coupled with oceanic variations.

✉ Jianping Li
ljp@ouc.edu.cn

1 College of Global Change and Earth System Science (GCESS), Beijing Normal University, Beijing 100875, China

2 Key Laboratory of Physical Oceanography-Institute for Advanced Ocean Studies, Ocean University of China and Qingdao National Laboratory for Marine Science and Technology, Qingdao 266100, China

3 Key Laboratory of Meteorological Disaster of Ministry of Education, Collaborative Innovation Center on Forecast and Evaluation of Meteorological Disasters, Institute for Climate and Application Research (ICAR), Nanjing University of Information Science and Technology, Nanjing 210044, China

4 State Key Laboratory of Numerical Modeling for Atmospheric Sciences and Geophysical Fluid Dynamics, Institute of Atmospheric Physics, Chinese Academy of Sciences, Beijing 100029, China

5 School of Earth Sciences, Zhejiang University, Hangzhou 310027, China

6 Center for Climate Physics, Institute of Basic Science, Busan, South Korea

7 Department of Atmospheric Sciences, Pusan National University, Busan, South Korea

1 Introduction

The Indian Ocean dipole (IOD), a fundamental mode of interannual climate variability (Saji et al. 1999; Webster et al. 1999), affects not only the climate in many countries surrounding the Indian Ocean rim, but also the global climate system; e.g., across eastern Africa, Indonesia, Australia, East Asia, and other regions, resulting in severe environmental and socioeconomic repercussions (Ashok et al. 2003, 2004; Guan and Yamagata 2003; Saji and Yamagata 2003; Cai et al. 2009; Li et al. 2011a, b). In light of these significant impacts, improving our understanding of the factors and processes that affect the development and evolution of IOD events is an urgent concern as it would improve our ability to predict the IOD and so mitigate the socioeconomic losses.

Observational and model results have demonstrated that IOD events can occur simultaneously with El Niño-Southern Oscillation (ENSO) events, and that the positive IOD is intimately linked to El Niño, but the negative IOD to La Niña (Xie et al. 2002; Annamalai et al. 2003; Krishnamurthy and Kirtman 2003; Behera et al. 2006; Huang and

Shukla 2007a; Schott et al. 2009; Yang et al. 2015; Zhang et al. 2015; Stuecker et al. 2017). Furthermore, during the boreal summer (June–July–August, JJA) and autumn (September–October–November, SON), the sea surface temperature anomalies (SSTAs) tend to be somewhat stronger around the western pole of the IOD (IOD-W) for the ENSO-induced IOD than for the independent IOD (Yu and Lau 2005; Behera et al. 2006). However, Huang and Shukla (2007b) indicated that the fluctuations of the Northwestern Pacific monsoon also play an important role in affecting the IOD during JJA by using the long-term simulations without ENSO forcing. More recently, Zhang et al. (2018) revealed that the South China Sea (SCS) summer monsoon (SCSSM), the remarkable interannual variability over the Northwestern Pacific Ocean, might also contribute to the IOD growth. Interestingly, the SCSSM strongly affects SSTAs around the eastern pole of the IOD (IOD-E) during JJA, and this is accompanied by weak SSTAs around the IOD-W, similar to the simulation results of Huang and Shukla (2007b). This leads us to question what differences exist between the effects of the SCSSM and ENSO on the IOD, particularly around the IOD-E and IOD-W. Thus, we explored the individual and combined effects of the SCSSM and ENSO on the IOD during JJA and SON, with the aim of uncovering the underlying physical mechanisms. Especially, we are concerned with the relationships between the SCSSM and IOD-E and between ENSO and IOD-W. In light of these physical processes, the SCSSM and JJA ENSO can improve substantially the seasonal predictive capacity of the IOD years during SON.

2 Datasets and methods

For this study, we used the monthly mean horizontal winds, vertical velocity, precipitation rate data, and surface heat flux (including surface sensible, latent, and radiation heat fluxes) for the period 1948–2015, gridded at a resolution of $2.5° \times 2.5°$. These data were obtained from the National Centers for Environmental Prediction-National Center for Atmospheric Research (NCEP/NCAR) reanalysis dataset (Kalnay et al. 1996). The improved Extended Reconstructed SST Version 5 (ERSST v5) data for the same period were on a $1° \times 1°$ grid (Huang et al. 2017). The subsurface temperature data were obtained from the Simple Ocean Data Assimilation (SODA, version 2.2.4) reanalysis dataset on a $0.5° \times 0.5°$ grid for the period 1948–2010, and used to calculate the heat content (Carton and Giese 2008). We removed the linear trend and the long-term (1948–2015) mean climatology from all datasets.

Niño-3.4 index, defined as the average of SSTAs in the region bounded by170°E–120°W and 5°N–5°S, was used to monitor ENSO variability and was derived from

NOAA Climate Prediction Center data (https://www.esrl. noaa.gov/psd/data/climateindices/list/). The strength of the IOD was measured by the dipole mode index (DMI), defined as the difference between the IOD-E index (EDMI) and IOD-W index (WDMI), which are defined as the SSTAs area-averaged over the southeastern Indian Ocean (90°–110°E, 10°S–0°) and western Indian Ocean (50°–70°E, 10°S–10°N), respectively (Saji et al. 1999). The DMI data were obtained from the Japan Agency for Marine-Earth Science and Technology (JAMSTEC; http://www.jamstec.go. jp/frcgc/research/d1/iod). The SCSSM index was calculated as the area-averaged summer (JJA) dynamical normalized seasonality for the 925-hPa wind field within the SCS monsoon domain (100°–125°E, 0°–25°N), and the wind data are available at http://ljp.gcess.cn/dct/page/65578 (Li and Zeng 2002, 2003; Li et al. 2010; Liu et al. 2017). The intensity of the SCSSM index is given by:

$$\delta = \frac{\|\bar{V}_1 - \mathrm{V}_{\mathrm{m,n}}\|}{\|\bar{V}\|} - 2,$$

where $\|*\|$ is a norm on the monsoon domain of integration, $\overline{V}1$ and $\overline{V}$ represent the January climatological wind vector and the mean of the January and July climatological wind vectors, respectively, and Vm, n denotes the monthly wind vectors in the mth month of the nth year.

The significance of correlations between variables X and Y was tested using a two-tailed Student's t test and the effective number of degrees of freedom (N_{eff}), which can be approximated as follows (e.g., Pyper and Peterman 1998; Li et al. 2013):

$$\frac{1}{N_{eff}} \approx \frac{1}{N} + \frac{2}{N} \sum_{i=1}^{N} \frac{N-j}{N} \rho_{XX}(j)\rho_{YY}(j),$$

where N indicates the total length of the time series, $\rho_{XX}(j)$ and $\rho_{YY}(j)$ represent the autocorrelations of two time series X and Y, respectively.

3 Three types of IOD

Figure 1 shows the scatterplots of the SON DMI with the SCSSM and JJA Niño-3.4 indices for the period 1948–2015. As shown in Fig. 1, the correlation coefficient between the SCSSM index (JJA Niño-3.4) and SON DMI is 0.57 (0.53) and exceeds the 99% confidence level based on a two-tailed Student's t-test using the effective number of degrees of freedom. This indicates that a strong (weak) SCSSM and El Niño (La Niña) are both intimately linked to positive (negative) IOD events (Fig. 1). However, we found that some IOD events occur simultaneously with both ENSO
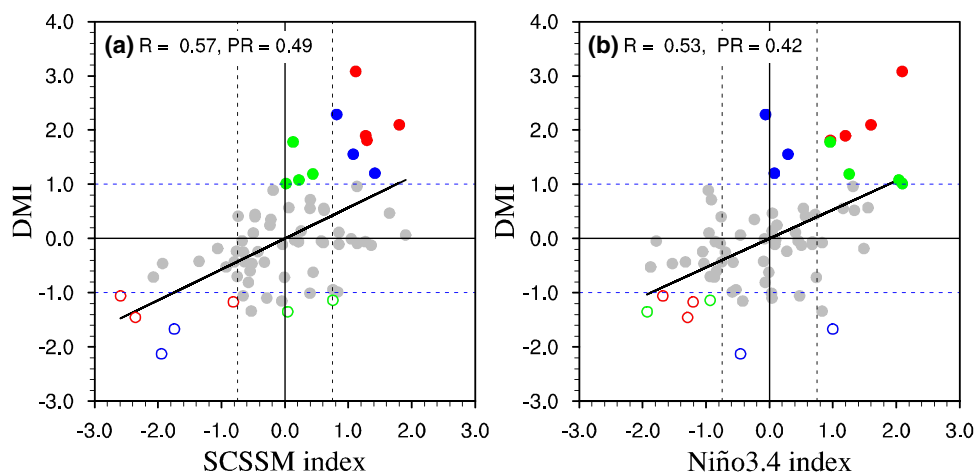
Fig. 1 Scatterplot of the SON DMI versus **a** the SCSSM index and **b** the JJA Niño-3.4 index. The red closed (open) dots indicate the positive (negative) IOD events that coincide with the strong (weak) SCSSM and El Niño (La Niña), and the blue closed (open) dots represent the positive (negative) IOD events that coincide with the strong (weak) SCSSM but with neutral ENSO events. The green dots are the same as the blue dots but with the reversed situation. R (PR) indicates the correlation (partial correlation) coefficients of the SON DMI with the SCSSM index (removing the JJA ENSO) and JJA Niño-3.4 index (removing SCSSM) beyond 99% confidence level, respectively. The black and blue dashed lines indicate the + 1 (− 1) standard deviation for IOD events and + 0.75 (− 0.75) standard deviations for SCSSM and JJA ENSO events, respectively

and SCSSM, and some other IOD events are associated with only the SCSSM or ENSO, which suggests that the SCSSM and JJA ENSO may have independent and combined influences on the SON IOD (Fig. 1). Partial correlation analysis also supports this interpretation; i.e., the SCSSM (JJA ENSO) remains significantly correlated with SON IOD, with a coefficient of 0.49 (0.45), after removing the JJA ENSO (SCSSM) signals (Fig. 1).

To further illustrate these issues, we classified 17 (of 21) IOD events that occurred between 1948 and 2015 and were closely associated with the SCSSM or ENSO into three types: the first type (hereafter IOD-Type I) is associated with both the SCSSM and ENSO, the second type (hereafter IOD-Type II) associated with only the SCSSM, and the third type (hereafter IOD-Type III) associated with only ENSO (Table 1). IOD (SCSSM and ENSO) events were defined as occurring when the absolute amplitude of the DMI (SCSSM and Niño-3.4 index) exceeded the 1 (0.75) standard deviation threshold during SON (JJA). Notably, the observed frequencies of occurrence of the IOD-Type I, IOD-Type II, and IOD-Type III events were 7/21, 5/21, and 5/21, respectively,

which is close to a ratio of 1:1:1 (as expected based on the nearly equal chance of occurrence for each tercile). In addition, there were further four IOD events (1960, 1980, 1992, and 2005) with neutral SCSSM and ENSO signals, but these were excluded from the present study.

Based on the three types of IOD (Table 1), it is reasonable to assume that the SCSSM and ENSO have both individual and combined effects on the IOD. We performed composite analysis based on the positive and negative phases of the IOD with respect to the three types of IOD that we defined and that occurred during our study period (1948–2015). Figure 2a and b show the composites for the DMI, IOD-E index (EDMI), and IOD-W index (WDMI) during JJA and SON, respectively, for the positive phase of the three types of IOD event. The DMI associated with IOD-Type I is larger than that associated with IOD-Types II and III during JJA and SON (Fig. 2a, b), suggesting a remarkable combined influence of the SCSSM and ENSO on IOD development. Li et al. (2019) recently provided a distinct definition and criteria of the combined effects, including synergistic and antagonistic effects. According to the definition and criteria

Table 1 Phases and classification of IOD years between 1948 and 2015

Classification	IOD-Type I	IOD-Type II	IOD-Type III
Positive IOD	1972, 1982, 1994, 1997	1961, 1967, 2006	1951, 1963, 1987
Negative IOD	1964, 1998, 2010	1958, 1996	1974, 1975

"IOD-Type I" is defined as occurring when a positive (negative) IOD event coincides with a strong (weak) SCSSM and El Niño (La Niña). "IOD-Type II" occurs when a positive (negative) IOD event coincides with a strong (weak) SCSSM but with an El Niño that is either neutral or has the opposite sign. "IOD-Type III" shows the reverse of the "IOD-Type II" pattern

Fig. 2 Composite of the DMI, EDMI, and WDMI in **a** JJA and **b** SON for the positive "IOD-Type I" (red), "IOD-Type II" (blue), and "IOD-Type III" (green) based on Table 1. **c**, **d** as **a**, **b**, but for the negative phases of three types IOD
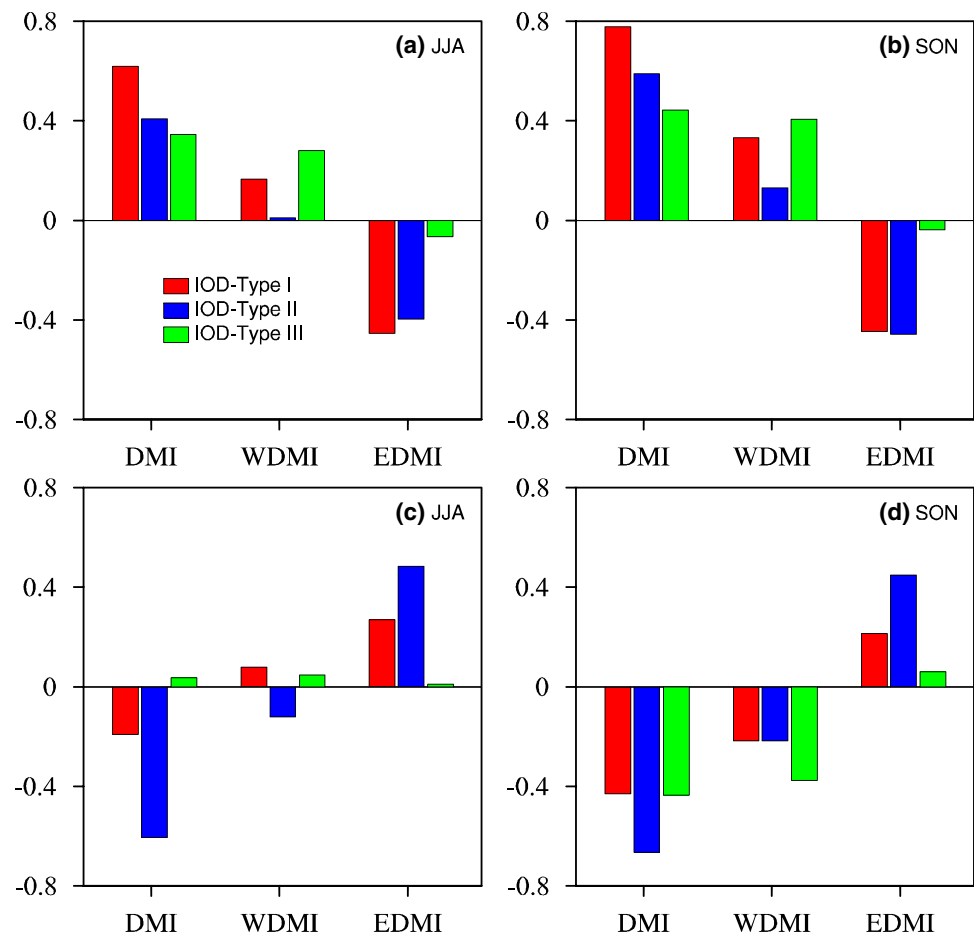
from Li et al. (2019), the intensity of the DMI related to both the SCSSM and ENSO is greater than that related to individual SCSSM/ENSO. More precisely, the combination of the SCSSM and ENSO has evident synergistic effect on the IOD. Meanwhile, IOD-W has a smaller amplitude than IOD-E during JJA, but a comparable amplitude during SON for IOD-Type I. However, for the positive IOD-Types II and III, there are distinct differences between IOD-E and IOD-W. In contrast to IOD-Type I, IOD-E is much more intense than IOD-W for IOD-Type II during JJA and SON, whereas the situation is reversed for IOD-Type III (Fig. 2a, b). The relationships during the negative phase are similar to those during the positive phase, but with the opposite sign (Fig. 2c, d). These findings suggest a closer relationship between the SCSSM and IOD-E, and also between ENSO and IOD-W, during JJA and SON.

These robust results were further verified using correlation analysis (Figs. 3, 4). The significant correlations between the SCSSM and the IOD persist from JJA to SON, whereas the correlation between the JJA ENSO and the IOD is only significant during SON (Fig. 3a, b), which is in agreement with the aforementioned studies (Zhang et al. 2018). We note that the significant correlations between the

SCSSM and IOD-E persist from JJA to SON, but have an insignificant correlation with IOD-W during JJA (Fig. 3a, b). Although the correlation between the SCSSM and IOD-W is significant during SON, it may be obscured by the ENSO signals during SON (Fig. 3c, d). In contrast, the JJA ENSO is significantly correlated with IOD-W during JJA and SON, whereas the correlation between the JJA ENSO and IOD-E is not significant (Fig. 3a, b).

To further examine the relationships among the SCSSM, JJA ENSO, IOD-E, and IOD-W, the correlation maps of the SCSSM and JJA ENSO with the SSTAs and 925-hPa wind anomalies during JJA and SON are shown in Fig. 4. The southwesterly anomalies over the SCS and western North Pacific and southeasterly anomalies over the tropical southeastern Indian Ocean are highly correlated with the SCSSM, accompanied with the cold SSTAs over the tropical southeastern Indian Ocean and comparable warm SSTAs over the tropical western Indian Ocean in JJA (Fig. 4a). This implies that the SCSSM may have stronger influences on the IOD-E than the IOD-W during JJA. In the following season, the southwesterly anomalies over the South China Sea and western North Pacific fade away followed by the demise of the SCSSM, while the southeasterly anomalies intensify and

Fig. 3 Correlation coefficients of the DMI, EDMI, and WDMI in **a** JJA and **b** SON with the SCSSM index ("R & SCSSM", orange bar) and the JJA Niño-3.4 index ("R & Niño-3.4", light blue bar) between 1948 and 2015. **c**, **d** as a, b, but for the partial correlation coefficients, e.g., "PR & SCSSM (Niño-3.4)" indicates the partial correlation coefficients of **c** JJA and **d** SON DMI, EDMI, and WDMI with the SCSSM (orange bar) (JJA Niño-3.4; light blue bar) index after removing JJA ENSO (SCSSM) signals during 1948–2015. The dashed lines in **a–d** indicate exceeding 99% confidence level, tested via a two-tailed Student's t-test using the effective number of degrees of freedom
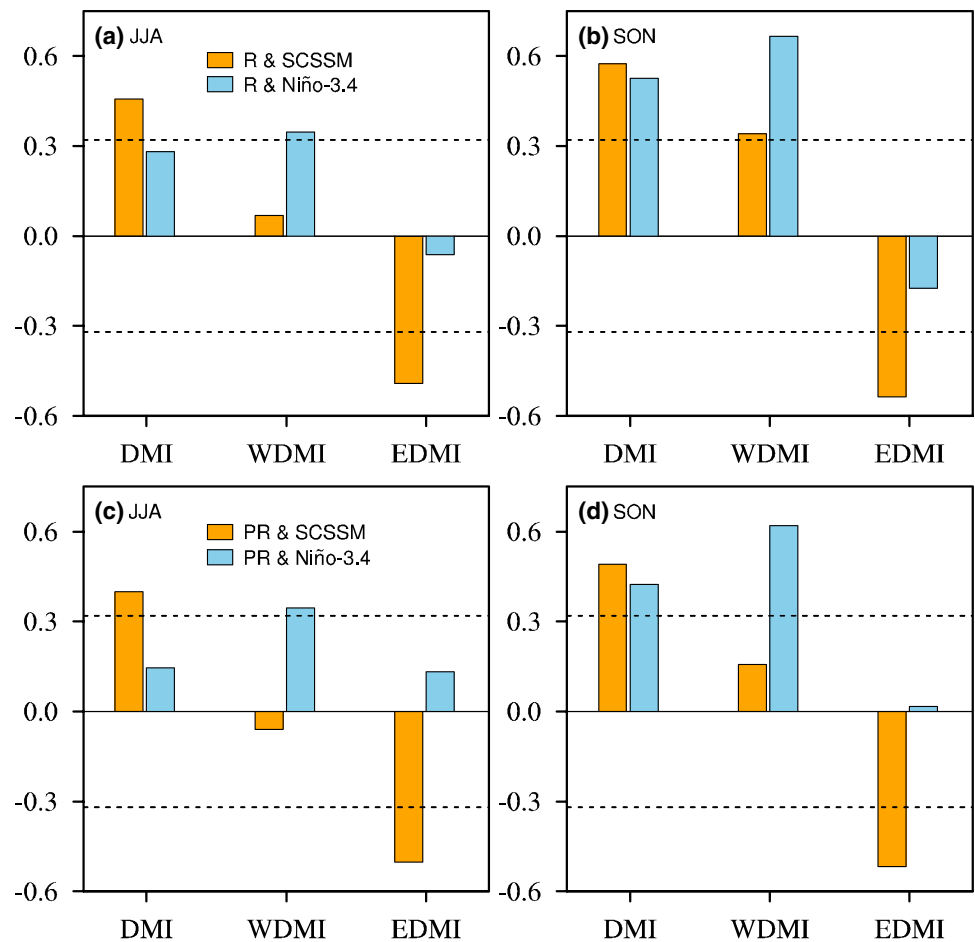
extend from the tropical southeastern Indian Ocean to western Indian Ocean (Fig. 4b). Correspondingly, the SSTAs strengthen rapidly over the tropical western Indian Ocean, accompanied by the enhancement of the cold SSTAs in the tropical southeastern Indian Ocean, which shows a remarkable peaking dipole feature during SON (Fig. 4b). Similarly, when ENSO develops in JJA, the evident southwesterly anomalies over the tropical western Pacific Ocean with the positive SSTAs in the tropical central eastern Pacific Ocean can be seen in Fig. 4c. Meanwhile, the positive SSTAs nearly cover over the entire tropical Indian Ocean basin during JJA, albeit with a weak SSTAs anomalies gradients between the tropical western central and southeastern Indian Ocean, accompanied with the weak southeasterly anomalies off Sumatra and Java coasts (Fig. 4c). With the growth of ENSO during SON, the SSTAs strengthen rapidly over the tropical western Indian Ocean, accompanied with the increased southeasterly anomalies over the tropical southeastern Indian Ocean (Fig. 4d). However, the SSTAs over the tropical southeastern Indian Ocean change slightly (Fig. 4d), indicating little influence of the JJA ENSO on the IOD-E.

Subsequently, the partial correlation analyses are further used to elucidate the aforementioned robust results

(Fig. 5). Figure 5a, b show the partial correlation maps of the SCSSM with the SSTAs and 925-hPa wind anomalies after removal the JJA ENSO signals. Compared with Fig. 4a, d, the correlations of the SCSSM with the SSTAs and 925-hPa wind anomalies are still significant over the tropical southeastern Indian Ocean and western North Pacific, while the correlations become insignificant over the tropical Pacific Ocean during JJA after excluding the JJA ENSO signals (Fig. 5a). Although the intensity of the SSTAs over the tropical Indian Ocean and southeasterly anomalies off Sumatra-Java during SON are weakened after removing the signals of the JJA ENSO, there exists the remarkable dipole feature over the tropical Indian Ocean, indicating the important influences of SCSSM on the IOD, especially for the IOD-E (Fig. 5b). In addition, the significant correlations over the tropical Pacific Ocean during SON disappear after removing the SON ENSO signals, and the correlations off Sumatra-Java are slightly weakened, yet still significant (not shown). Hence, the significant SSTAs over the tropical Pacific Ocean in Fig. 5b may result from SON ENSO. In contrast to JJA ENSO, the southeasterly anomalies off Sumatra-Java disappear after removal the signals of the SCSSM in JJA, while the SSTAs
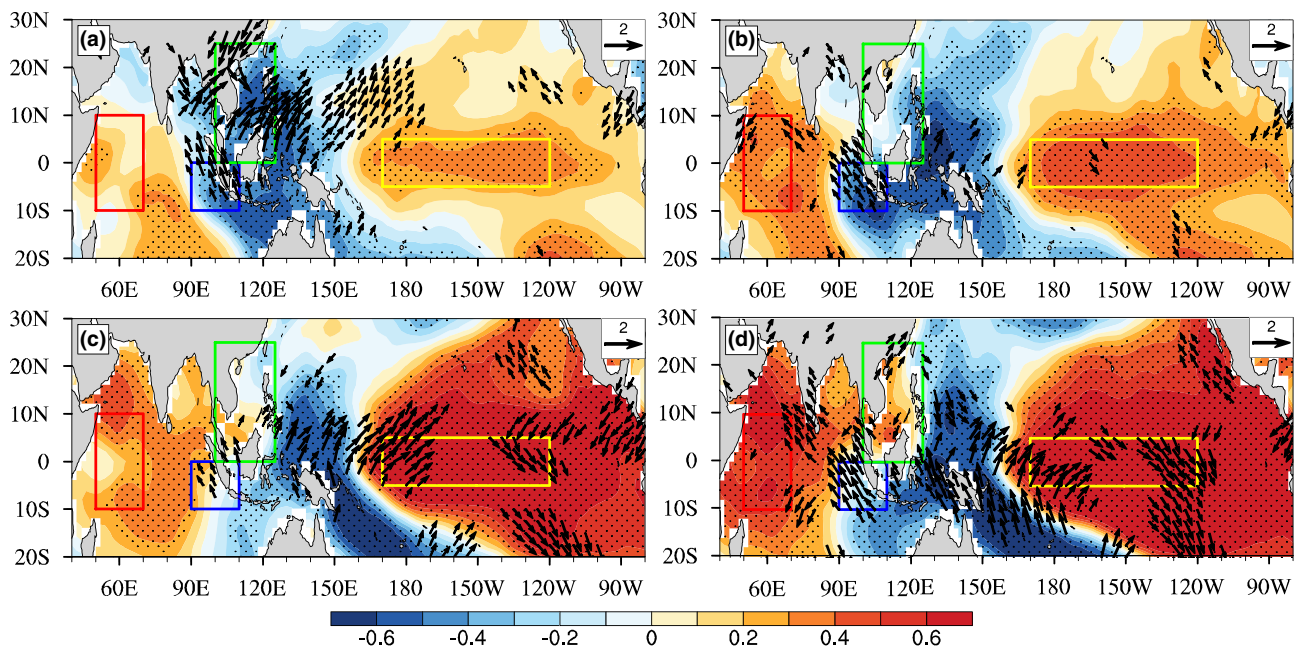
Fig. 4 Correlations of the SCSSM index with SSTAs (shading) and wind anomalies (vectors) at 925–hPa during JJA (**a**) and SON (**b**); **c**, **d** as in **a**, **b**, but for the JJA Niño-3.4 index. The green and yellow rectangles in **a–d** denote the SCSSM (100°–125°E, 0°–25°N) and Niño-3.4 index (170°E–120°W, 5°S–5°N) region, respectively. Blue and red rectangles as the green and yellow rectangles in **a–d**, but for the tropical southeastern Indian Ocean (90°–110°E, 10°S–0°), western Indian Ocean (50°–70°E, 10°S–10°N). Black stipples indicate 95% confidence level, and only wind vectors that are significant at the 95% confidence are plotted
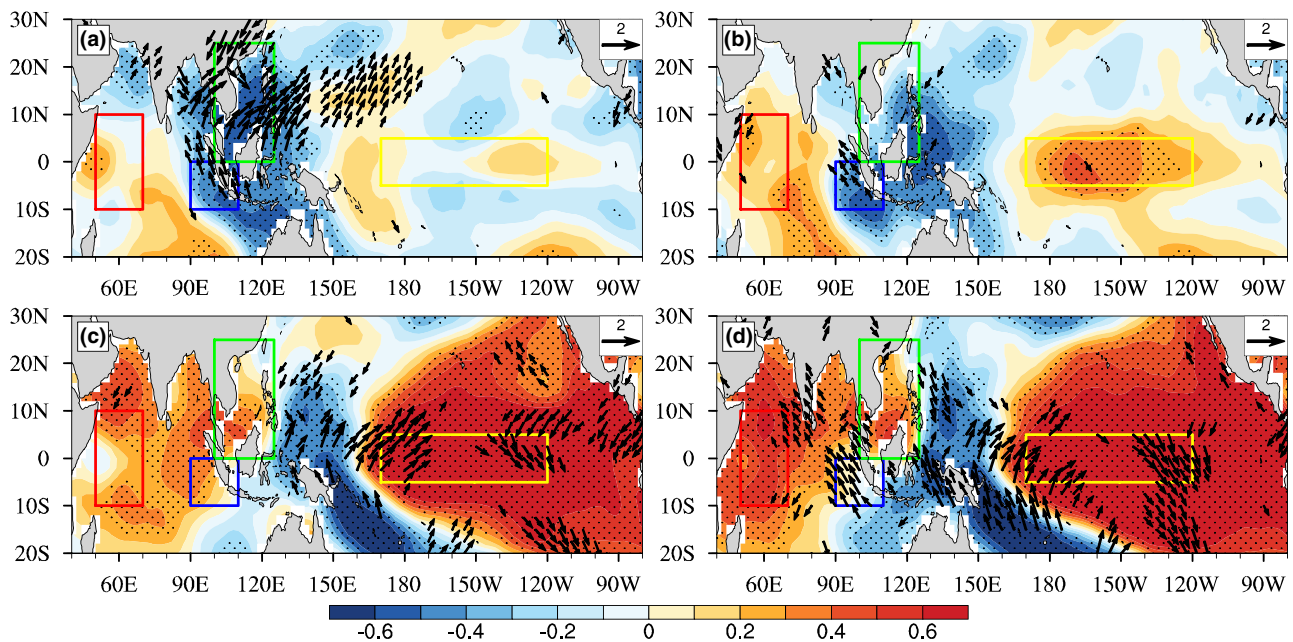
Fig. 5 Same as Fig. 4, but for the partial correlations after removing the JJA ENSO (**a**, **b**) and SCSSM signals (**c**, **d**)

over the tropical Pacific and Indian Ocean are slightly weakened (Fig. 5c). This implies the prominent effect of the SCSSM on IOD-E. In SON, the relationships of the JJA ENSO with the SSTAs and 925-hPa wind anomalies are as apparent as in Fig. 4d, indicating the bare influence of the SCSSM on the IOD-W (Fig. 5d).

Overall, based on the composite and correlation analyses, the SCSSM and JJA ENSO both favor the development of

the IOD, whereas IOD-E (IOD-W) is affected mainly by the SCSSM (ENSO) during JJA and SON. This leads us to question how the SCSSM (ENSO) affects IOD-E (IOD-W).

4 Possible physical mechanism

The atmospheric circulation coupled with oceanic dynamic processes, acting as a "coupled oceanic-atmospheric bridge" proposed recently by Li et al. (2019), plays an essential role of the SCSSM in affecting the IOD through the positive wind–thermocline–SST (Bjerknes) and wind–evaporation–SST (WES) feedbacks (Zhang et al. 2018). IOD-Types I and II are associated with the SCSSM and have a similar magnitude of easterly and southerly wind anomalies at roughly 110°E during JJA, but these anomalies are much stronger than those of IOD-Type III, which is associated with only ENSO (Fig. 6a, b). An important pathway by which the SCSSM enhances the southeasterly wind anomalies off Sumatra and Java may be the anomalous precipitation dipole (Fig. 7a, b) and SCSSM Hadley circulation (Fig. 8a, b; i.e.,

the 'SCSSM Hadley circulation' of Zhang et al. 2018) over the western North Pacific and southern Maritime Continent during JJA. As has been shown previously (Zhang et al. 2018; Huang and Shukla 2007b), the southeasterly wind off the Sumatra–Java coast, serving as a crucial component of the positive Bjerknes and WES feedbacks, plays a key role in IOD formation during JJA. The enhanced southeasterly wind induced by the SCSSM not only increases the excessive surface evaporation and latent heat flux loss from the ocean, but also tends to lift the local thermocline anomalies and bring colder subsurface water to the surface (Fig. 6a–d). This suggests a greater latent heat flux loss from the ocean and reduced ocean heat content over IOD-E for IOD-Types I and II during JJA, which contributes to the colder SSTAs there (Fig. 6c, d). In contrast, the weaker southeasterly wind anomalies of IOD-Type III correspond to the weaker SSTAs off the coasts of Sumatra and Java during JJA (Fig. 6e).

The anomalous SCSSM Hadley circulation and precipitation dipole disappear when the SCSSM withdraws during SON (Figs. 7d, e, 8d, e), whereas the increased zonal gradient of SSTAs associated with IOD-Type II leads to a
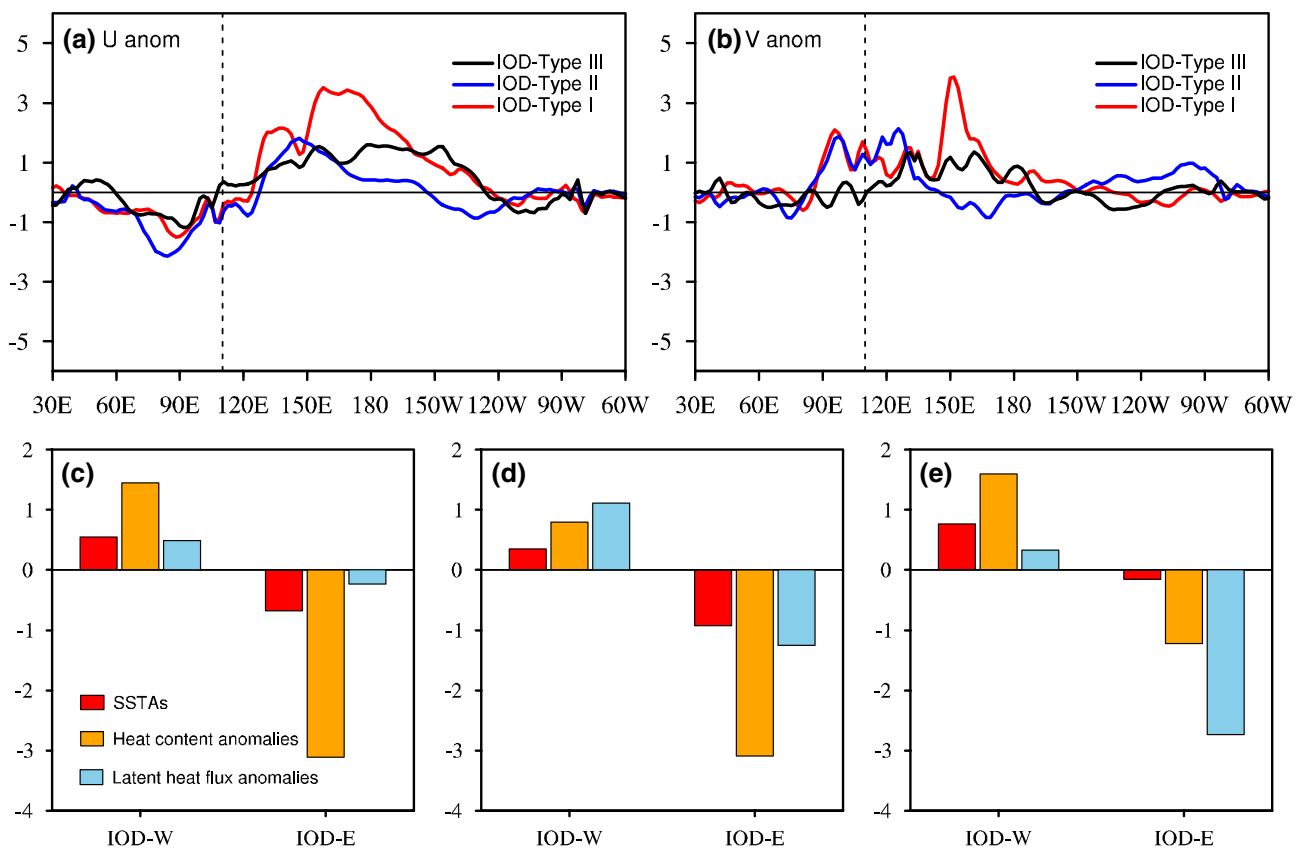
Fig. 6 **a** Composite of the zonal wind anomalies (U anom, m s^{-1}) averaged between 10°S and 0° for "IOD-Type I", "IOD-Type II", and "IOD-Type III" during JJA. **b** As in **a**, but for the meridional wind anomalies (V anom, m s^{-1}). The vertical dashed line in **a**, **b** is located at 110°E. Composite of the SSTAs (red, °C), heat content anoma- lies (orange, 10^8 J m^{-2}), and latent heat flux anomalies (sky blue, 10 W m^{-2}) for **c** "IOD-Type I", **d** "IOD-Type II", and **e** "IOD-Type III" during JJA. Positive (negative) latent heat flux anomalies indicate heat gain by the ocean (atmosphere)
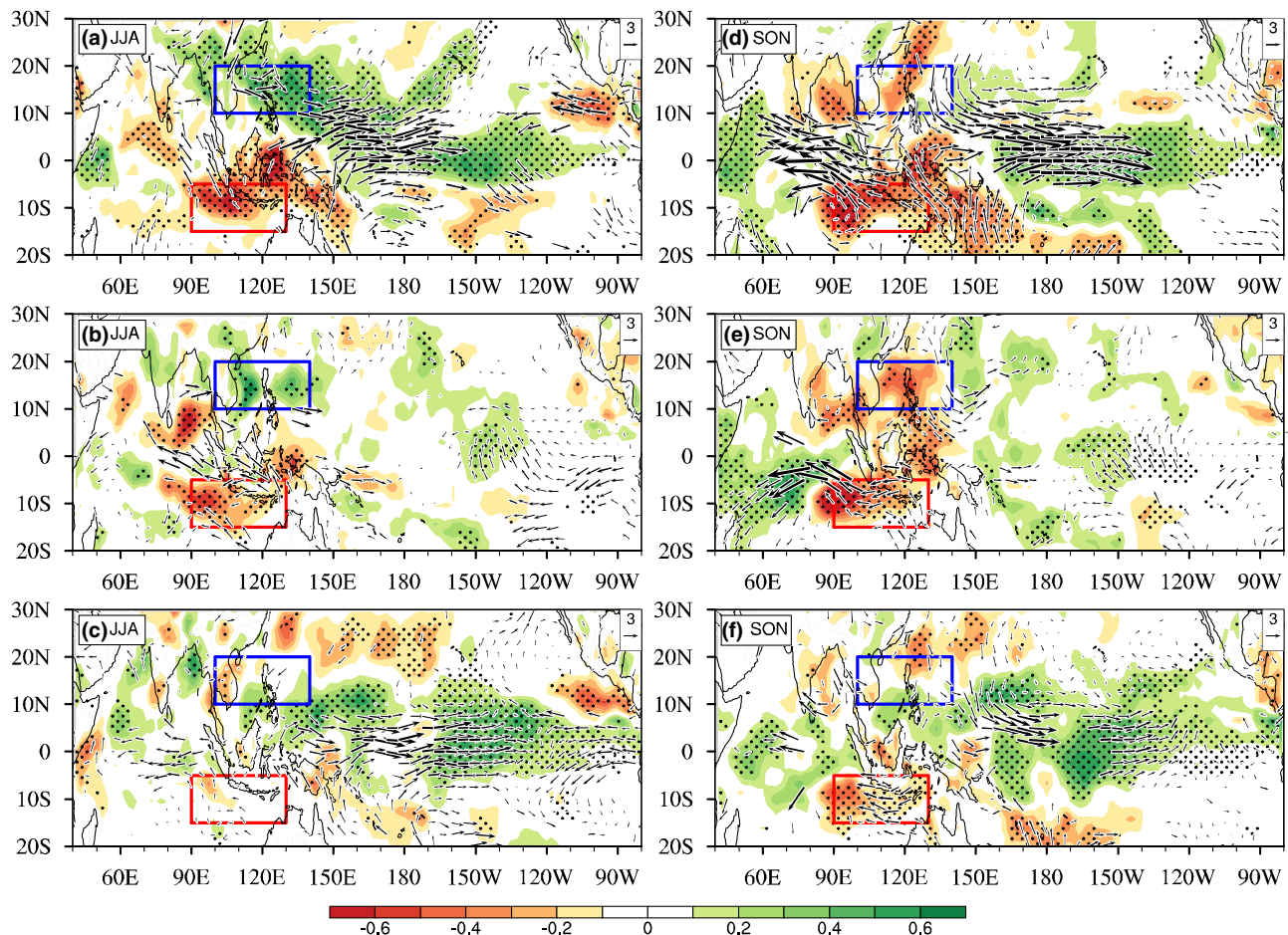
Fig. 7 Composite difference in the precipitation rate (shading, kg m^{-2} s^{-1}) and 925-hPa wind (vector, m s^{-1}) anomalies for **a** "IOD-Type I", **b** "IOD-Type II", and **c** "IOD-Type III" during JJA. **d**, **e**, and **f** as in **a**, **b**, **c** but during SON. Black stipples and vectors in **a**–**f** indicate that the composite anomalies are statistically significant at the 90% confidence level. The red and blue rectangles in **a**–**f** indicate the study areas over the western North Pacific (100°–140°E, 10°–20°N) and southern Maritime Continent (90°–130°E, 15°–5°S), respectively

stronger equatorial easterly wind than that associated with IOD-Type III (Fig. 9a). This increased equatorial easterly contributes to the enhancement of SSTAs over IOD-E and IOD-W by changing the ocean heat content and latent heat flux anomalies within the framework of a positive Bjerknes feedback (Fig. 9d), especially for IOD-Type II.

However, this physical pathway is not suitable for IOD-Type III, which is associated only with ENSO, because the precipitation anomalies show the same sign over the western North Pacific and southern Maritime Continent (Fig. 7c, f) and the anomalous SCSSM Hadley circulation breaks up during JJA and SON (Fig. 8c, f). Now that the pathway by which ENSO affects the IOD is not via the SCSSM Hadley circulation from JJA to SON, and then how ENSO does affect the IOD remains topic of great interest.

The Walker circulation, which is sensitive to the SSTAs over the tropical Pacific and Indian Ocean, serves as the "atmospheric bridge" by which ENSO affects the IOD, as described in previous studies (Klein et al. 1999; Wang and Wang 2014; Zhang et al. 2015). For IOD-Type I, both the central-eastern tropical Pacific Ocean and western Indian Ocean SSTAs have loadings of the same sign, whereas those of the tropical Indo-Pacific region are opposite during JJA (Fig. 10a). As the atmospheric response, two separate upward flows occur simultaneously over the tropical western Indian and central Pacific, accompanied by downward flow near 120°E (Fig. 11a). Corresponding to the anomalous descending motion, a strong anomalous divergence is anchored over the Indo-western Pacific region in the lower troposphere (Fig. 12a). The surface southeasterly anomalies near Sumatra and Java are effective in favoring oceanic upwelling and thermocline tilting in the tropical southeastern Indian Ocean, which results in cold SSTAs there. The surface easterly and southerly anomalies over the tropical central Indian Ocean become stronger (Fig. 9a, b) as the anomalous Walker circulation induced by the enhanced El
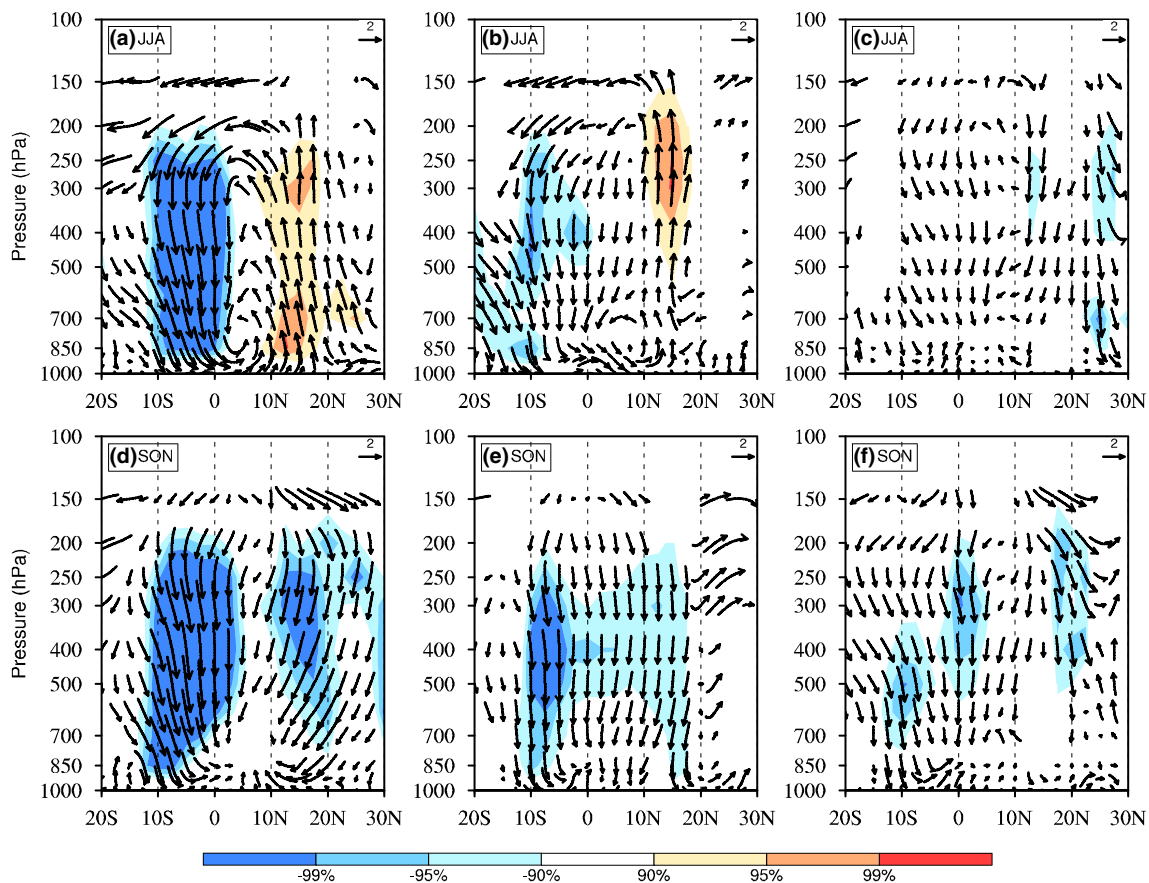
Fig. 8 Composite differences of the meridional–vertical circulation anomalies averaged between 90°E and 140°E (vector, m s^{-1}) for **a**, **d** "IOD-Type I", **b**, **d** "IOD-Type II", and **c**, **f** "IOD-Type III" during JJA (**a**–**c**) and SON (**d**–**f**). Shading in **a**–**f** indicates vertical pressure velocity anomalies (-10^{-2} Pa s^{-1})

Niño increases during SON (Fig. 10d, 11d), favoring the enhancement of the cold SSTAs off the Sumatra–Java coast. The positive SSTAs thereby intensify and cover the tropical central and western Indian Ocean via the positive Bjerknes feedback, which indicates a dramatic peaking of these features during SON (Figs. 9c, 10d).

By comparison, a similar SSTAs dipole pattern appears in the tropical Indian Ocean but with insignificant SSTAs over the tropical Pacific Ocean during JJA for IOD-Type II (Fig. 10b). Although we also find the weak atmospheric response associated with the descending motion to the west of 120°E (Fig. 11b) and lower-level divergence over the Indo-Pacific region (Fig. 12b), it may be induced mainly by the anomalous SCSSM Hadley circulation during JJA (Fig. 8b). The increased zonal gradient of SSTAs from JJA to SON leads to the development of a single Walker circulation over the tropical Indian Ocean, and this strengthens the surface easterly anomalies over the tropical central Indian Ocean during SON (Fig. 11e), leading to the dramatic peaking of the SSTAs dipole pattern (Figs. 9d, 10e).

For IOD-Type III, the large positive SSTAs over the tropical central-eastern Pacific Ocean and the tropical central Indian Ocean are significantly related to El Niño, and are accompanied by weak negative SSTAs in the tropical southeastern and western Indian Ocean during JJA (Fig. 10f). The westerly anomalies offset the prevailing easterly anomalies near 60°E (Fig. 6a), leading to evaporative cooling and then against warming SSTAs to the west of 60°E (Fig. 6e). Although the latent heat flux anomalies over IOD-W for IOD-Type III associated with ENSO are smaller than those for IOD-Type II associated with the SCSSM during SON, the stronger SSTAs over IOD-W occurs during IOD-Type III, and is determined mainly by the change in ocean heat content anomalies related to ENSO (Fig. 9e). In contrast to IOD-Type I, which is related to both the SCSSM and ENSO, an evident descending motion to the east of 60°W (Fig. 11f) and lower-level divergence occur during IOD-Type III, which is related only to ENSO over the tropical Atlantic Ocean (Fig. 12f), and implies another possibility; i.e., that ENSO affects IOD-W via the tropical Atlantic Ocean.
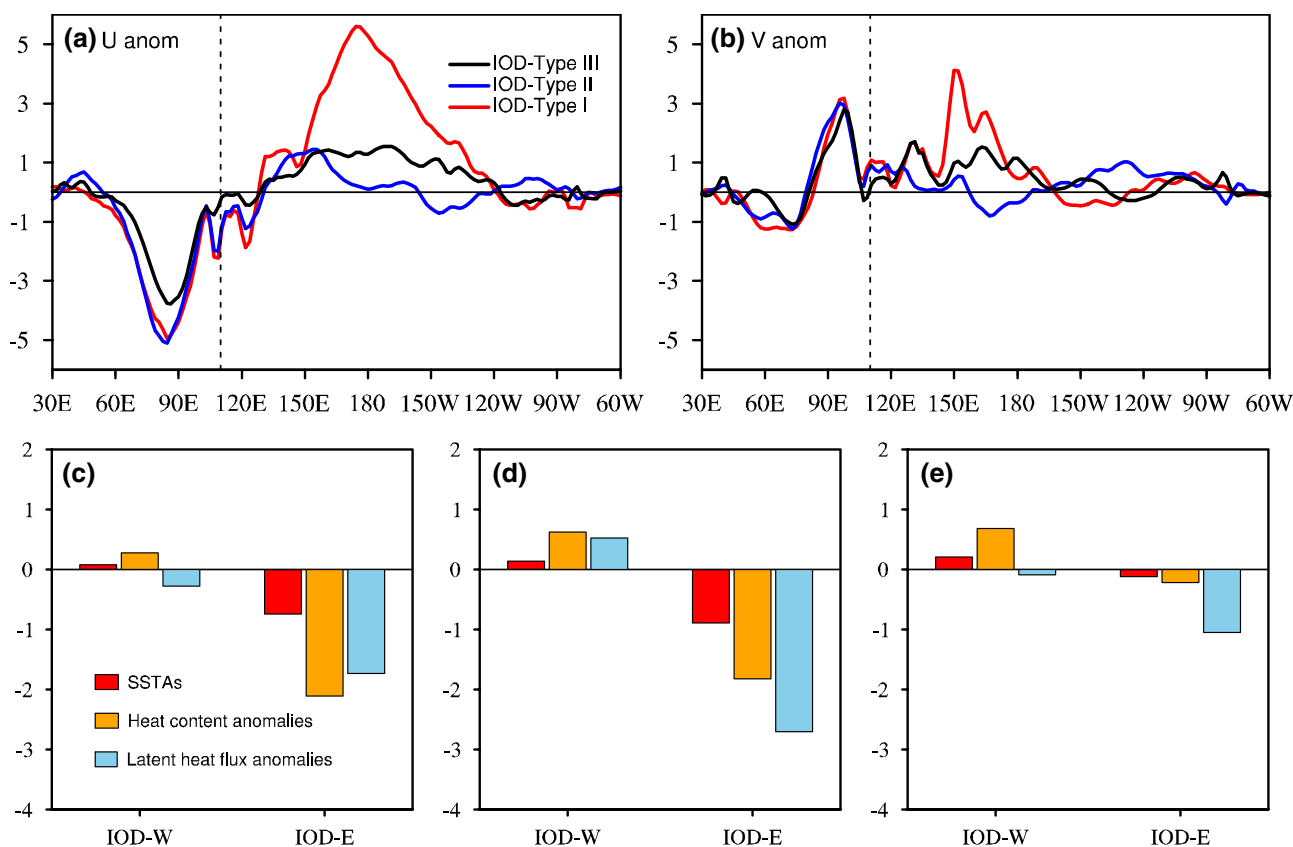
Fig. 9 Same as Fig. 6, but during SON

Due to the weaker intensity of El Niño associated with IOD-Type I, although the significant ascending branch induced by the warm SSTAs over the tropical Pacific Ocean is centered at 160°W during JJA, the descending branch of the Walker circulation near 120°E is much weaker (Figs. 10c, 11c), consist with Zhang et al. (2015). This weak Walker circulation is not effective in contributing to either the surface easterly anomalies (Fig. 6a), or to the southerly anomalies off the coasts of Sumatra and Java (Fig. 6b), thereby leading to moderately cold SSTAs near Sumatra and Java during JJA. Similarly, two Walker circulations, but of lower intensity, are found over the tropical Pacific and Indian oceans during SON (Fig. 10f). In contrast to IOD-Types I and II, the descending motion and equatorial surface easterly anomalies over the tropical Indian Ocean are much weaker (Fig. 9a), albeit with similar amplitude of the surface southerly over the tropical southeastern Indian Ocean (Fig. 9b), resulting in smaller contributions to the development of IOD-E.

The aforementioned results have interpreted the underlying physical mechanism of the SCSSM and ENSO affecting the IOD. The simultaneous SCSSM imprints its signal on the SSTAs over IOD-E during JJA through the "atmospheric bridge", i.e., the anomalous precipitation dipole and SCSSM

Hadley circulation, and then the enhanced SSTAs over IOD-E, acting as the "oceanic bridge" (referred to Nan and Li 2005a, b), contribute to the enhancement of the SSTAs over IOD-W via the positive Bjerknes feedback. The formed dipole over the tropical Indian Ocean persists and peaks in the subsequent season based on the oceanic-atmospheric process. Similarly, the Walker circulation induced by ENSO first plays the "atmospheric bridge" in linking between the IOD and ENSO and then is coupled with the oceanic process, favoring the mature of the IOD during the ensuing season. Overall, although the pathways of the SCSSM and ENSO impacting on the IOD are quite different, the amplitude of the SSTAs over IOD-E and IOD-W are essentially determined by the SCSSM and ENSO through the "coupled ocean-atmospheric bridge" (reviewed by Li et al. 2019), respectively.

5 Discussion and conclusions

In summary, the SCSSM and ENSO have remarkable individual and synergistic effects on the IOD. When the positive IOD is closely linked to both the strong SCSSM and El Niño (IOD-Type I), significant cool SSTAs develop over the
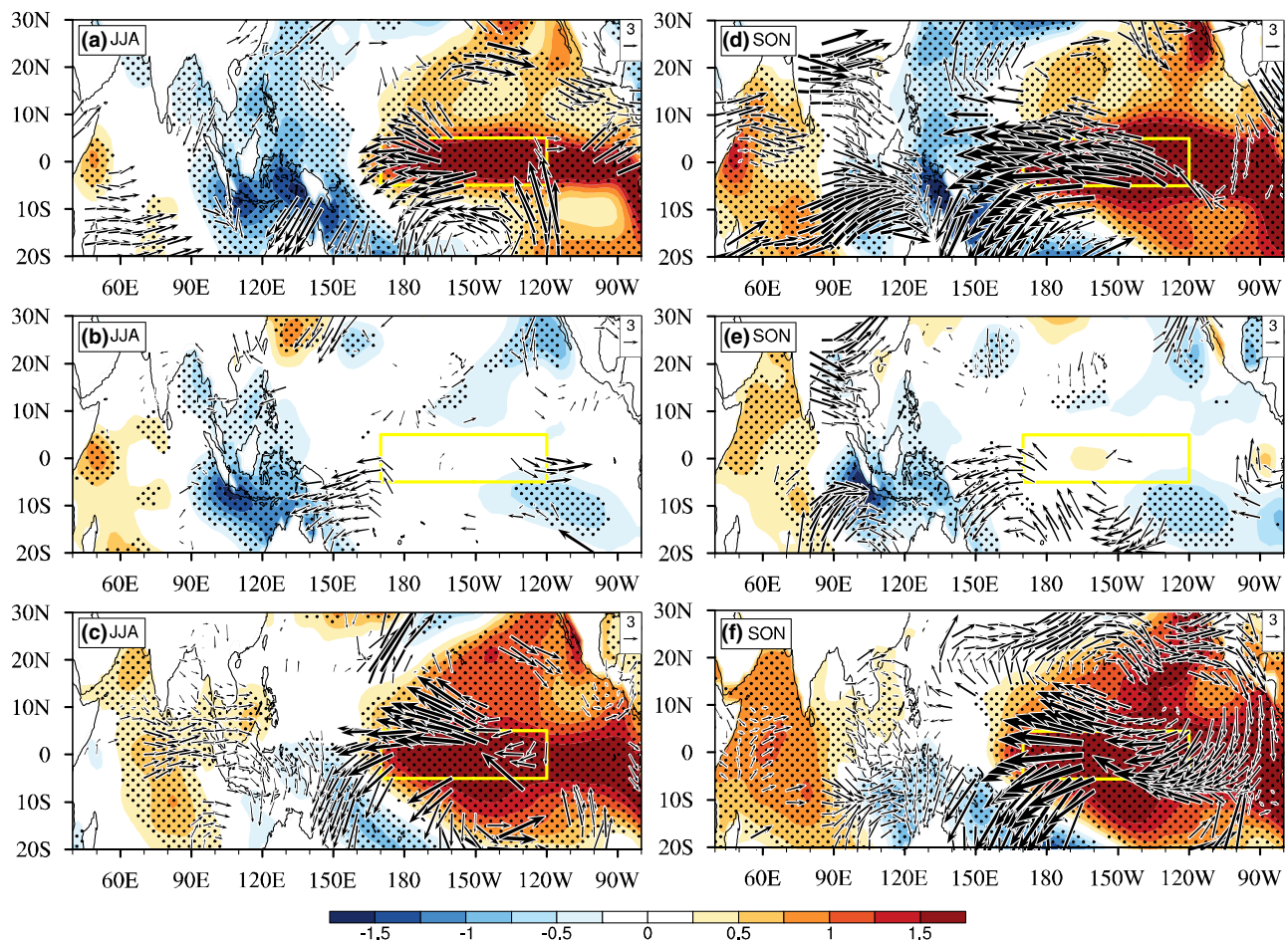
Fig. 10 Same as Fig. 7, but for the SSTAs (shading, °C) and 200-hPa wind (vector, m s^{-1}) anomalies for **a**, **d** "IOD-Type I", **b**, **d** "IOD-Type II", and **c**, **f** "IOD-Type III" during JJA (**a**–**c**) and SON (**d**–**f**)

tropical southeastern Indian Ocean and warm SSTAs over the western Indian Ocean during JJA and SON, corresponding to the remarkable equatorial easterly wind anomalies over the tropical Indian Ocean. This pattern describes the typical evolution of positive IOD events, with the situation reversed in their negative counterparts. The pattern associated with IOD-Type II is similar to that of IOD-Type I, but with weaker warm SSTAs over a smaller area of the tropical western Indian. The anomalous SCSSM Hadley circulation favors subsidence and a further reduction of precipitation over the tropical southeastern Indian Ocean, which leads to the cooling of the SSTAs off the coasts of Sumatra and Java through the positive Bjerknes and WES feedbacks during JJA. Even if the SCSSM withdraws during SON, IOD-Type II is able to persist and reach a peak during SON with the assistance of the positive Bjerknes feedback. IOD-Type III is also similar to IOD-Type I, but with weaker SSTAs off the Sumatra–Java coast. The anomalous Walker circulation is constrained over the tropical Pacific Ocean due to the weak El Niño during JJA. As El Niño intensifies through

SON, the enhanced Walker circulation favors descending motion over the southern Maritime Continent and ascending motion over the tropical western Indian Ocean, resulting in warmer SSTAs over the tropical western Indian Ocean and weak cooling off the Sumatra–Java coast. The weak SSTAs off the Sumatra–Java coast may be limited by the weakened equatorial easterly wind anomalies associated with the weaker ENSO. In summary, the intensity of the SSTAs over IOD-E and IOD-W are essentially affected by the SCSSM and ENSO via the "coupled ocean-atmospheric bridge", respectively. The physical processes that facilitate the impact of the SCSSM and SON ENSO on the IOD are shown schematically in Fig. 13.

The aforementioned results have demonstrated that the SCSSM and ENSO have both individual and synergistic effects on the IOD during JJA and SON. Actually, there are remarkable differences for three types of IOD events during the following winter (December–January–February, DJF) and spring (March–April–May, MAM). The SSTAs of the IOD-Type II related to SCSSM show a dipole pattern
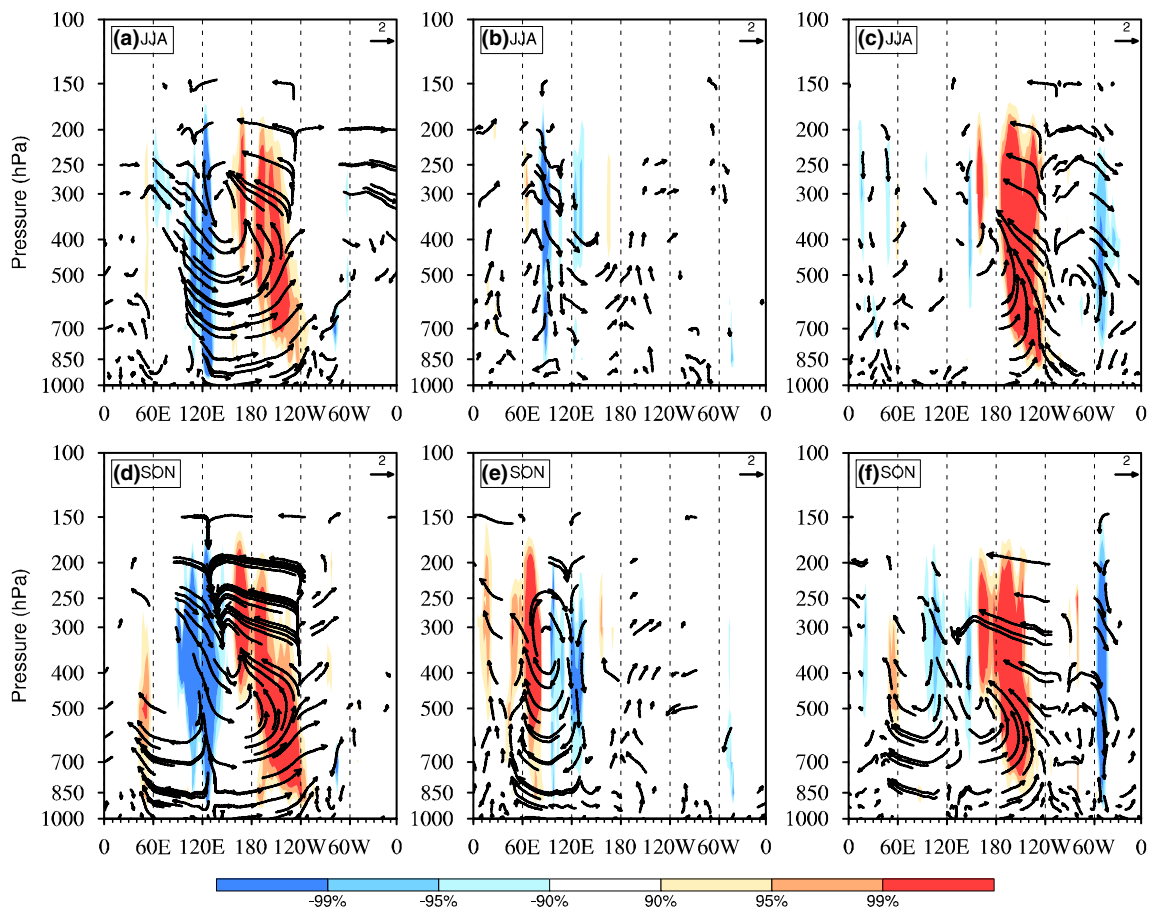
Fig. 11 As in Fig. 8, but for zonal-vertical circulation anomalies averaged between 5°S and 5°N (vector, m s^{-1}) and vertical pressure velocity anomalies (shading, -10^{-2} Pa s^{-1}) for **a, d** "IOD-Type I", **b, d** "IOD-Type II", and **c, f** "IOD-Type III" during JJA (**a–c**) and SON (**d–f**)

over the tropical Indian Ocean during the following DJF and MAM, but with the smaller scale and weaker intensity (e.g., Huang and Kinter 2002; Fig. 14b, e). However, as the El Niño peaks in DJF, the positive SSTAs of the IOD-Type III related to ENSO cover the whole basin Indian Ocean (Fig. 14c), the so-called Indian Ocean basin-wide mode (IOBM), and persist until MAM (Fig. 14f). This may be attributed to the longer persistence of ENSO than the SCSSM. Similar to the IOD-Type I, the SSTAs of the IOD-Type III related to both SCSSM and ESNO also experience a IOBM during the following DJF and MAM, but with a larger amplitude (Fig. 14a, d), implying the possible synergistic effects of the SCSSM and ENSO on the amplitude of the IOBM in the following MAM.

Besides, the remarkable differences in SSTAs over the tropical Pacific Ocean exist between the IOD-Type I and IOD-Type III both related to ENSO during the following MAM. Quite different from the warm SSTAs over the tropical Pacific Ocean for the IOD-Type I during MAM (Fig. 14d), the cold SSTAs associated with the IOD-Type III develop and extend from the coast of Peru to the equatorial

central Pacific, showing a La Niña pattern (Fig. 14f). Ha et al. (2016) demonstrated that the combined effects of the IOD during the developing El Niño phase and the IOBM during the decaying phase facilitate rapid termination of El Niño and transition to La Niña by modulating the easterly wind anomalies over the eastern Indian and western Pacific Oceans, similar to the situation in IOD-Type III. As indicated by Ha et al. (2016), now that the SSTAs of the IOD-Type I and IOD-Type III related to ENSO over the tropical Indian Ocean resemble qualitatively, why does not La Niña develop over the tropical Pacific Ocean for the IOD-Type I? Notably, the amplitude of the SSTAs for the IOD-Type III over the tropical Atlantic Ocean is much stronger than that related to IOD-Type I. This implies that the SSTAs over the tropical Atlantic Ocean may play a potential role in modulating the effect of the combination of the IOD and IOBM on ENSO phase transition, which is worthy of further inquiring thoroughly.

In addition, when the IOD coincides with ENSO (IOD-Types I and III), the amplitude of the positive phase is evidently stronger than the negative phase, especially during
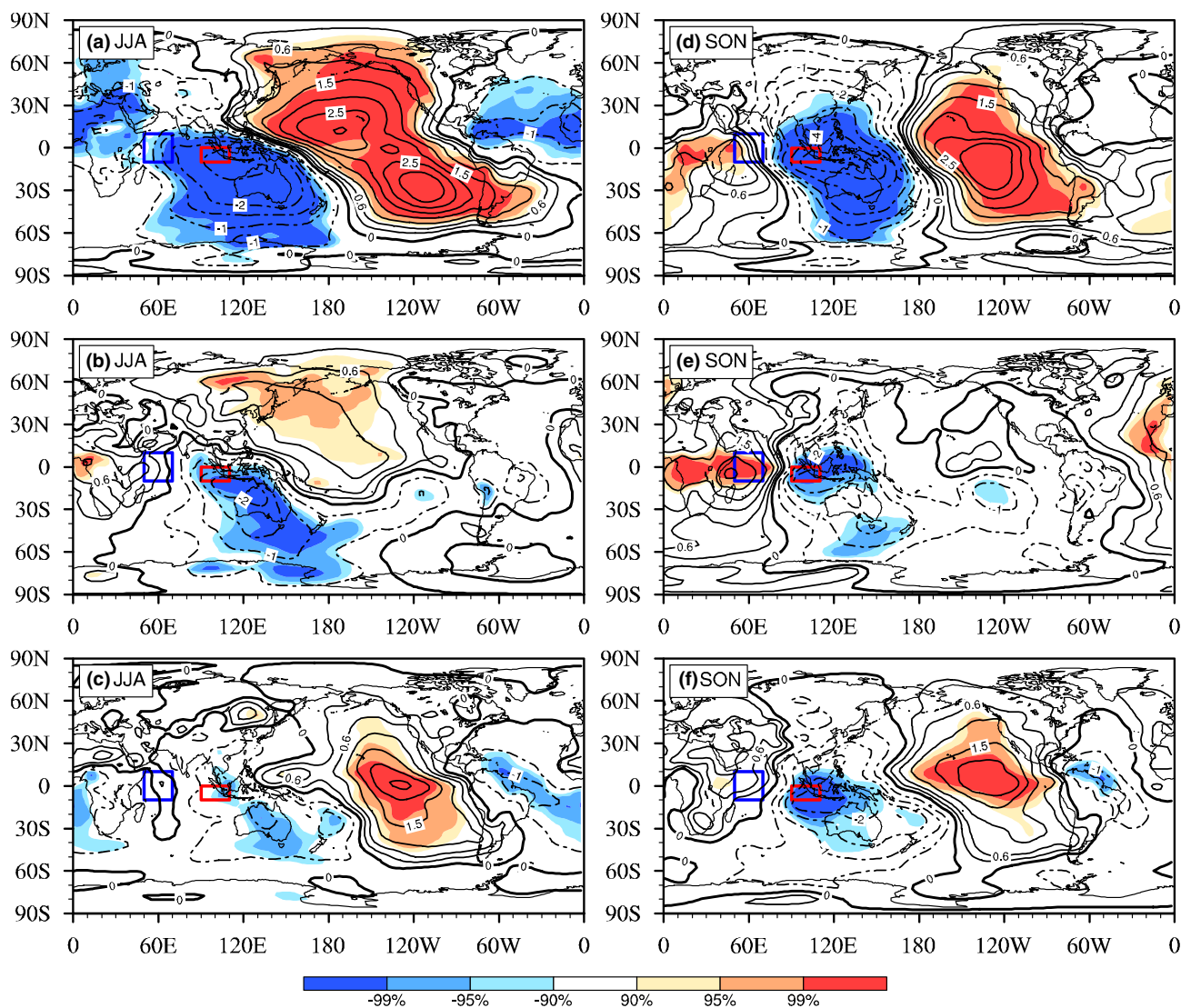
Fig. 12 As in Fig. 7, but for 925 hPa velocity potential anomalies (counter, 10^6 m^2 s^{-1})

JJA, but this situation is reversed for IOD-Type II, which is associated only with the SCSSM (Fig. 2). This may be the limited numbers of positive and negative IOD events. Another possible reason for the asymmetry between positive and negative IOD phases may be the asymmetric ENSO–Indian Ocean coupling with respect to El Niño and La Niña; i.e., El Niño events are usually stronger than La Niña events (An and Jin 2004; Kug et al. 2006). Nevertheless, these asymmetries do not disturb the dominant

influence of the SCSSM (ENSO) around IOD-E (IOD-W) described in this study.

In addition to the 17 IOD events analyzed in this study, there were four IOD events (1960, 1980, 1992, and 2005) that were associated with neither the SCSSM nor ENSO, and this indicates that other external impact factors, such as the southern annular mode (Lau and Nath 2004), Indo-Pacific warm pool (Annamalai et al. 2003; Song et al. 2007), and the Indonesian throughflow (Tozuka et al. 2007), should be taken take into consideration in future studies.
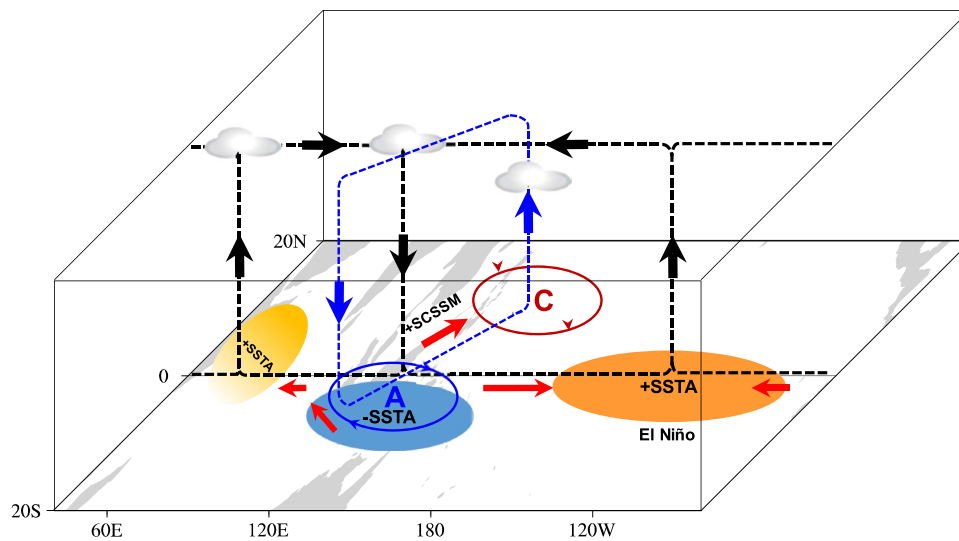
Fig. 13 Schematic diagram of the SCSSM (JJA) and ENSO (SON) affecting the IOD. "+" indicates the significant positive SSTAs, strong SCSSM, and "−" indicates the negative SSTAs. The red vectors represent the condition for the strong SCSSM or El Niño. The cloud indicates the positive precipitation anomalies over the tropi-cal central-eastern Pacific, western North Pacific and western Indian Ocean, and the black (blue) circulation line with the black (blue) vectors denotes the anomalous Walker (Hadley) circulation. The red (blue) elliptic circle with the arrows denotes the anomalous cyclone (C) or anticyclone (A)
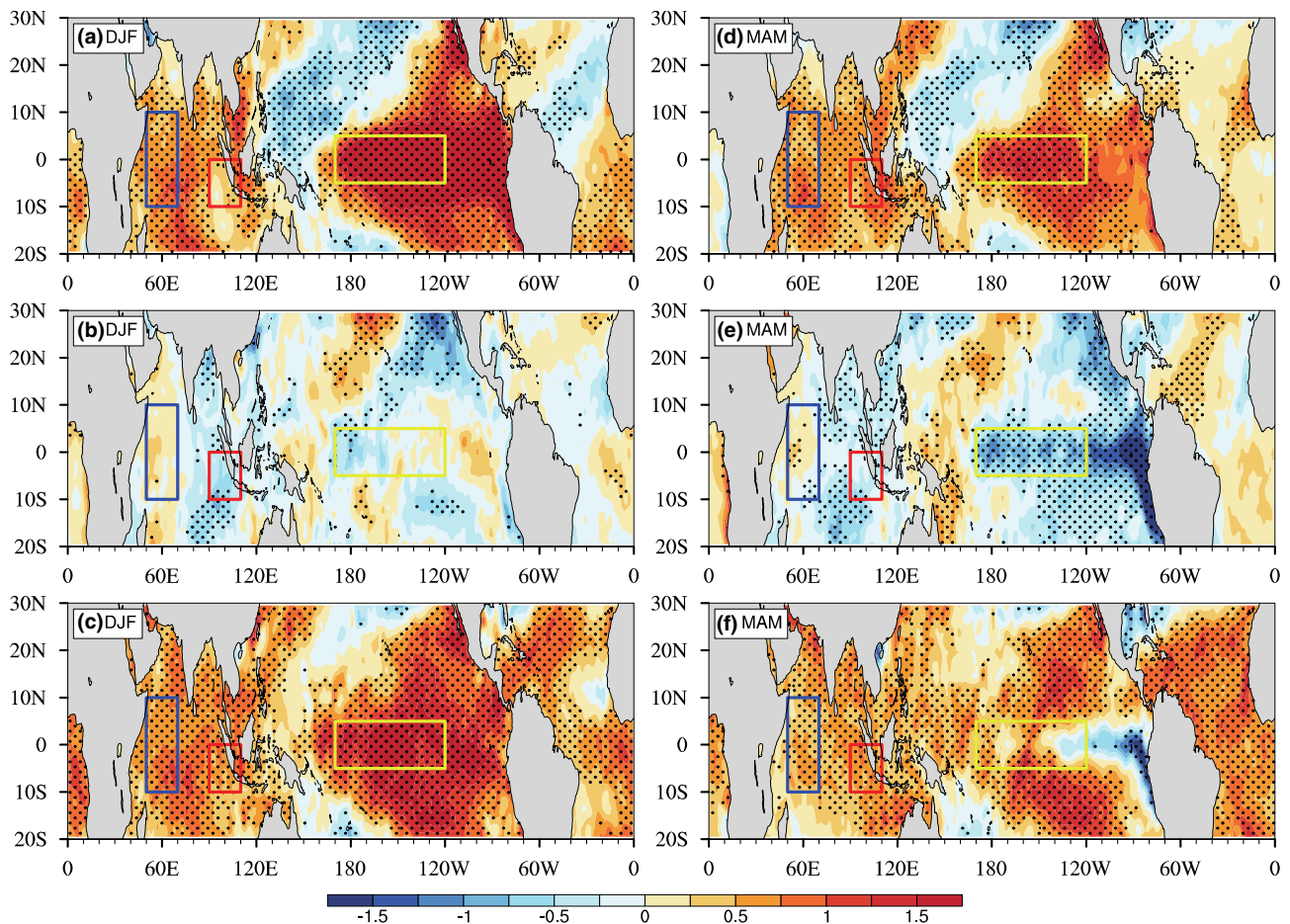
Fig. 14 Same as Fig. 10, but for **a**, **d** "IOD-Type I", **b**, **d** "IOD-Type II", and **c**, **f** "IOD-Type III" during the following DJF (**a**–**c**) and MAM (**d**–**f**)

References

An SI, Jin FF (2004) Nonlinearity and asymmetry of ENSO. J Clim 17:2399–2412. https://doi.org/10.1175/1520-0442(2004)017%3c2399:NAAOE%3e2.0.CO;2

Annamalai H, Murtugudde R, Potemra J, Xie SP, Liu P, Wang B (2003) Coupled dynamics over the Indian Ocean: Spring initiation of the zonal mode. Deep Sea Res Part II 50:2305–2330. https://doi.org/10.1016/S0967-0645(03)00058-4

Ashok K, Guan Z, Yamagata T (2003) Influence of the Indian Ocean dipole on the Australian winter rainfall. Geophys Res Lett. https://doi.org/10.1029/2003gl017926

Ashok K, Guan Z, Saji N, Yamagata T (2004) Individual and combined influences of ENSO and the Indian Ocean dipole on the Indian summer monsoon. J Clim 17:3141–3155. https://doi.org/10.1175/1520-0442(2004)017%3c3141:IACIOE%3e2.0.CO;2

Behera SK, Luo JJ, Masson S, Rao SA, Sakuma H, Yamagata T (2006) A CGCM study on the interaction between IOD and ENSO. J Clim 19:1688–1705. https://doi.org/10.1175/JCLI3797.1

Cai W, Cowan T, Sullivan A (2009) Recent unprecedented skewness towards positive Indian Ocean Dipole occurrences and its impact on Australian rainfall. Geophys Res Lett. https://doi.org/10.1029/2009GL037604

Carton JA, Giese BS (2008) A reanalysis of ocean climate using Simple Ocean Data Assimilation (SODA). Mon Weather Rev 136:2999–3017. https://doi.org/10.1175/2007MWR1978.1

Guan ZY, Yamagata T (2003) The unusual summer of 1994 in East Asia: IOD teleconnections. Geophys Res Lett 30:51.51–51.54. https://doi.org/10.1029/2002GL016831

Ha KJ, Chu JE, Lee JY, Yun KS (2016) Interbasin coupling between the tropical Indian and Pacific Ocean on interannual timescale: observation and CMIP5 reproduction. Clim Dyn 48:459–475

Huang BH, Kinter JL (2002) Interannual variability in the tropical Indian Ocean. J Geophys Res 107(C11):20-1–20-26

Huang BH, Shukla J (2007a) Mechanisms for the interannual variability in the tropical Indian Ocean. Part I: the role of remote forcing from the tropical Pacific. J Clim 20(13):2917–2936

Huang BH, Shukla J (2007b) Mechanisms for the interannual variability in the tropical Indian Ocean. Part II: regional processes. J Clim 20(13):2937–2960

Huang BY, Thorne PW, Banzon VF, Boyer T, Zhang HM (2017) Extended reconstructed sea surface temperature, version 5 (ersstv5): upgrades, validations, and intercomparisons. J Clim 30(20):8179–8205. https://doi.org/10.1175/JCLI-D-16-0836.1

Kalnay E, Kanamitsu M, Kistler R, Collins W, Deaven D, Gandin L, Iredell M, Saha S, White G, Woollen J (1996) The NCEP/NCAR 40-year reanalysis project. Bull Am Meteorol Soc 77:437–471. https://doi.org/10.1175/1520-0477(1996)077%3c0437:TNYRP%3e2.0.CO;2

Klein SA, Soden BJ, Lau NC (1999) Remote sea surface temperature variations during ENSO: evidence for a tropical atmospheric bridge. J Clim 12:917–932. https://doi.org/10.1175/1520-0442(1999)012,0917:RSSTVD.2.0.CO;2

Krishnamurthy V, Kirtman BP (2003) Variability of the Indian Ocean: Relation to monsoon and ENSO. Q J R Meteorol Soc 129:1623–1646. https://doi.org/10.1256/qj.01.166

Kug JS, Kang IS, Li T, An SI, Kirtman BP (2006) Role of ENSO-Indian ocean coupling on ENSO variability. Geophys Res Lett 33:268–269. https://doi.org/10.1029/2005GL024916

Lau NC, Nath MJ (2004) Coupled GCM simulation of atmosphere–ocean variability associated with zonally asymmetric SST changes in the tropical Indian Ocean. J Clim 17:245–265. https://doi.org/10.1175/1520-0442(2004)017%3c0245:CGSOAV%3e2.0.CO;2

Li JP, Zeng QC (2002) A unified monsoon index. Geophys Res Lett 29(8):115

Li JP, Zeng QC (2003) A new monsoon index and the geographical distribution of the global monsoons. Adv Atmos Sci 20:299–302

Li JP, Wu ZW, Jiang Z, He J (2010) Can global warming strengthen the East Asian summer monsoon? J Clim 23:6696–6705

Li JP, Wu GX, Hu DX (2011a) Ocean-atmosphere interaction over the joining area of Asia and Indian-Pacific ocean and its impact on the short-term climate variation in China (in Chinese), vol 1. China Meteorological Press, Beijing, p 516

Li JP, Wu GX, Hu DX (2011b) Ocean–Atmosphere interaction over the joining area of Asia and Indian-Pacific ocean and its impact on the short-term climate variation in China (in Chinese), vol 2. China Meteorological Press, Beijing, p 565

Li JP, Sun C, Jin FF (2013) NAO implicated as a predictor of Northern Hemisphere mean temperature multi-decadal variability. Geophys Res Lett 40:5497–5502

Li JP, Zheng F, Sun C, Feng J, Wang J (2019) Pathways of influence of the Northern Hemisphere mid-high latitudes on East Asian climate: a review. Adv Atmos Sci 36:902–921. https://doi.org/10.1007/s00376-019-8236-5

Liu T, Li J J, Li Y, Zhao S, Zheng F, Zheng J, Yao Z (2017) Influence of the May Southern annular mode on the South China Sea summer monsoon. Clim Dyn 51:1–13

Nan SL, Li JP (2005a) The relationship between the summer precipitation in the Yangtze River valley and the boreal spring Southern Hemisphere annular mode: I Basic facts. Acta Meteorol Sinica 63(6):837–846. https://doi.org/10.3321/j.issn:0577-6619.2005.06.001 **(in Chinese with English abstract)**

Nan SL, Li JP (2005b) The relationship between the summer precipitation in the Yangtze River valley and the boreal spring Southern Hemisphere annular mode: II The role of the Indian Ocean and South China Sea as an "oceanic bridge". Acta Meteorol Sinica 63(6):847–856. https://doi.org/10.11676/qxxb2005.081 **(in Chinese with English abstract)**

Pyper BJ, Peterman RM (1998) Comparison of methods to account for autocorrelation in correlation analyses of fish data. Can J Fish Aquat Sci 55:2127–2140

Saji N, Yamagata T (2003) Possible impacts of Indian Ocean dipole mode events on global climate. Clim Res 25:151–169. https://doi.org/10.3354/cr025151

Saji N, Goswami B, Vinayachandran P, Yamagata T (1999) A dipole mode in the tropical Indian Ocean. Nature 401:360–363. https://doi.org/10.1038/43854

Schott FA, Xie SP, McCreary JP (2009) Indian Ocean circulation and climate variability. Rev Geophys. https://doi.org/10.1029/2007RG000245

Song Q, Vecchi GA, Rosati AJ (2007) Indian Ocean variability in the GFDL coupled climate model. J Clim 20:2895–2916. https://doi.org/10.1175/JCLI4159.1

Stuecker MF, Timmermann A, Jin FF, Chikamoto Y, Zhang W, Wittenberg AT, Widiasih E, Zhao S (2017) Revisiting ENSO/Indian

Ocean dipole phase relationships. Geophys Res Lett 44:2481–2492. https://doi.org/10.1002/2016GL072308

Tozuka T, Luo JJ, Masson S, Yamagata T (2007) Decadal modulations of the Indian Ocean dipole in the SINTEX-F1 coupled GCM. J Clim 20:2881–2894. https://doi.org/10.1175/JCLI4168.1

Wang X, Wang C (2014) Different impacts of various El Niño events on the Indian Ocean Dipole. Clim Dyn 42:991–1005

Webster PJ, Moore AM, Loschnigg JP, Leben RR (1999) Coupled ocean–atmosphere dynamics in the Indian Ocean during 1997–98. Nature 401:356–360

Xie SP, Annamalai H, Schott FA, McCreary JP Jr (2002) Structure and mechanisms of South Indian Ocean climate variability. J Clim 15:864–878

Yang Y, Xie SP, Wu L, Kosaka Y, Lau N-C, Vecchi GA (2015) Seasonality and predictability of the Indian Ocean dipole mode: ENSO forcing and internal variability. J Clim 28:8021–8036

Yu JY, Lau KM (2005) Contrasting Indian Ocean SST variability with and without ENSO influence: a coupled atmosphere-ocean GCM study. Meteorol Atmos Phys 90:179–191

Zhang W, Wang Y, Jin F-F, Stuecker MF, Turner AG (2015) Impact of different El Niño types on the El Niño/IOD relationship. Geophys Res Lett 42:8570–8576

Zhang YZ, Li JP, Xue JQ, Feng J, Wang QY, Xu YD, Wang YH, Zheng F (2018) Impact of the South China Sea summer monsoon on the Indian Ocean dipole. J Clim 31:6557–6573